PLANE STRAIN COMPRESSION TESTS WITH IMAGE ANALYSIS ON DENSE TOYOURA SAND

Job MUNENE KARIMI[1], Junichi KOSEKI[2] and Takeshi SATO[3]

ABSTRACT: A series of monotonic, cyclic and creep drained plane strain compression tests were performed on fully saturated samples of dense Toyoura sand at a confining pressure of 49kPa. Comparisons were made among monotonic, cyclic and creep plane strain compression tests to determine the differences on the peak strength of specimens with and without cyclic or creep loading history. To study strain localization characteristics and their relation with the failure mechanism of dense Toyoura sand, strain distributions were calculated based on image analysis of digital photographs taken at different stages of loading during each test. Several significant observations on the characteristics of strain localization could be made from the data.

Key Words: Strain localization, sand, drained shear, peak strength, shear band, cyclic loading, creep loading, plane strain compression tests, image analysis

INTRODUCTION

In the performance-based design used for designing large-scale structures such as retaining walls, the behavior of geo-materials, such as the backfill, under large earthquake loads needs to be well understood in order to guarantee a secure but cost-effective design. For example, the 1995 Hyogoken-Nambu earthquake caused serious damage to conventional masonry and concrete gravity type retaining walls for railway embankments. On the other hand, the reinforced soil retaining walls exhibited a ductile behavior and did not reach critical failure. (Tatsuoka et al., 1996). The subsoil reaction and seismic earth pressure of the backfill of a retaining wall are affected by the dynamic interaction between the wall and the subsoil/backfill. The detailed mechanisms have not yet been well understood.

Accurate knowledge of the failure mechanism and the behavior of a geo-material under large amplitude cyclic loading, such as earthquake load, are necessary. This is the basis of the present research. The influence of large amplitude cyclic loading on the strength and deformation properties of dense sand, and in particular its strain localization behavior, is not well understood. The experimental data on this study is scarce.

Koseki et al., (1998a, 1999) conducted both tilting and sinusoidal shaking table tests on different retaining wall models with Toyoura sand as the backfill. Both residual displacement of the wall and residual deformation of the backfill were investigated. They observed that although the failure plane was formed in a similar manner in both tests, the wall displacement in the tilting tests when the failure plane was formed was much smaller than that in the shaking table tests. This indicates that the condition of formation of failure plane under static loading is largely different from that under dynamic loading. They also observed that localized shear displacements accumulated in the backfill only along a single failure plane. Similar element tests are conducted in this study to compare with the results from the above tilting and sinusoidal shaking model tests.

[1] Formerly graduate student, Department of Civil Engineering, University of Tokyo
[2] Professor, Institute of Industrial Science, University of Tokyo
[3] Research Associate, Institute of Industrial Science, University of Tokyo

Later Watanabe et al. (2003) performed a series of model tests on the same retaining wall models to compare their performance during irregular shaking. The results from irregular shaking tests were compared with those from tilting tests and sinusoidal shaking tests as reported by Koseki et al. (1998a, 1999). They observed that, for the cantilever type retaining wall, two different failure planes developed almost simultaneously. On the other hand in the leaning and gravity type retaining walls, the first failure plane developed much earlier than the second failure plane. Koseki et al. (1998b) concluded that this progressive formation of multiple failure planes can be explained by effects of strain localization in the backfill soil and associated post peak reduction in the shear resistance from peak to residual values along the previously formed failure plane. Although the elemental tests conducted in this research are with constant amplitude of cyclic stress, the observed properties on strain localization will provide useful information on formation of shear banding in the above model tests.

Experimental studies have been conducted to investigate the behaviour of sand under plane strain condition by several researchers including Masuda et al. (1999) who performed compression, extension and cyclic loading tests on sand, Tatsuoka et al. (1990) who studied strength anisotropy and shear band direction on sand, Yoshida et al. (1994) on shear banding of sands, Oda et al. (1978) on anisotropic shear strength of sand, Arthur and Assadi (1977) on ruptured sand sheared in plane strain and Lam and Tatsuoka (1987) who investigated the effects of initial anisotropic fabric on strength and deformation behaviour of sand. Since the strain localization properties of dense sand under large amplitude cyclic loading are not well understood, a series of plane strain compression tests were performed in the present study on saturated specimens of air-pluviated Toyoura sand.

In addition, since the strain localization properties of dense sand under creep loading are not well understood, creep loading tests under plane strain compression were also performed in th is study.

MATERIAL, APPARATUS AND TEST PROCEDURES

The test material is Toyoura sand, Batch G (e_{max}=0.961, e_{min}=0.601, G_s=2.635). Toyoura sand is a quartz-rich sieved Japanese sand, which originates from weathered granite at Toyoura, Yamaguchi prefecture. The particles are angular to sub-angular in the grain shape and almost uniformly graded. Toyoura sand has been extensively used in element and model tests in Japan. eg., Tatsuoka et al., (1986,1990), AnhDan et al. (2002), among others. Throughout these studies, Toyoura sand has been established as a standard material for research to understand the behavior of granular media.

The test specimen and its stress states are shown in Fig. 1. The test specimen was prepared first by pluviating dry sand particles through air into a horizontal mould. This was followed by wetting, draining and freezing the specimen. The test conditions were as follows: (a) angle of vertical loading relative to bedding plane (δ)=0^0, (b) effective confining stress (σ_3') by vacuum = 49kPa, (c) initial relative density (D_r)=90%, (d) vertical loading from isotropic stress state under drained condition and (e) saturated specimens. It should be noted that specimens with vertical bedding planes were prepared by rotating frozen specimens with horizontal bedding planes by 90 degrees.

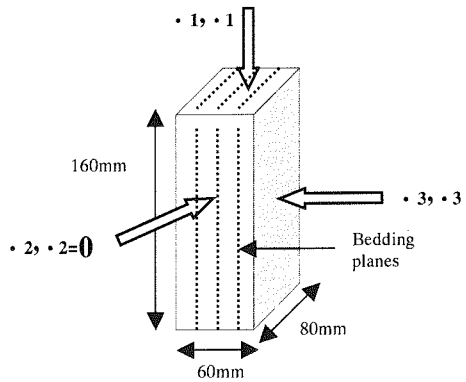

Figure 1 Prismatic specimen and stress states

The apparatus employed is a small-scale plane strain compression (PSC) apparatus shown in Fig. 2 (Salas Monge et al., 2002). It consists of a triaxial cell with a capacity of 3MPa, a cell pressure system, hydraulic axial loading system and a data acquisition system. The axial displacement is controlled by a hydraulic loading system, which is free from backlash when changing the loading direction. Axial loads are measured using a load cell with a capacity of 9.8kN, located inside the triaxial cell and hence free from errors due to piston friction (Tatsuoka 1988). The effective pressure is measured with a high capacity differential pressure transducer (HCDPT). Strains in the principal directions are measured locally using proximity transducers and local deformation transducers (LDT). All transducers are connected to amplifiers and after passing a low pass filter, the voltage values are converted to digital values and recorded by the computer. A feedback system using a digital to analog converter (D/A) is employed to control the axial load and cell pressure. This allows the desired stress paths to be followed automatically.

For performing plane strain compression (PSC) tests, a lateral restraining system was used. The lateral load is measured with a load cell attached between one of the confining platens and the end plate. One of the confining platens is made of a well-polished transparent plexiglass, which allows the deformation of the whole specimen to be observed accurately. To ensure smooth lateral displacement of the confining platens, both the stiffening frame and the end platen are supported by four small sliding rollers, which are sitting on the base of the triaxial cell. Friction force is measured with two additional load cells and vertical stresses are corrected accordingly. To allow the movement in σ_3 direction that is necessary for free development of a single shear band with a plane parallel to σ_2 direction, the pedestal is mounted on a moving plate, which in turn is lying on a set of two ball bearings.

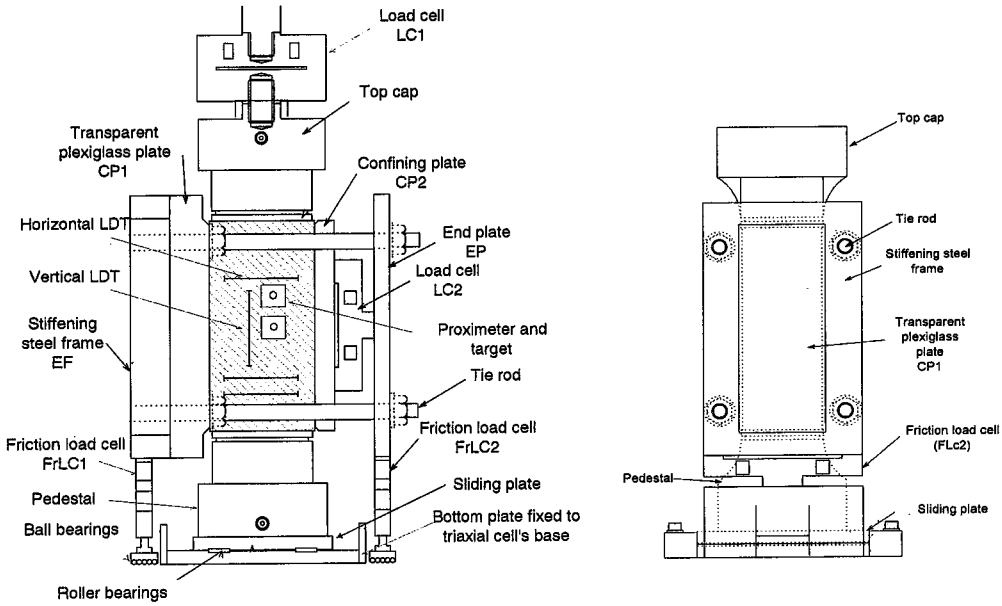

Figure 2. Lateral and front views of the plane strain compression (PSC) testing apparatus.

All principal strains of the tested material were measured locally. Both local deformation transducers and proximeters (gap sensors) were used. Local deformation transducers (LDTs) (Goto et al.1991) consist of a thin phosphor bronze strip with strain gauges glued to the central part of it on opposite sides. They are capable of detecting changes in length between their two ends. Their ends are fixed to two hinges, which are in turn attached to the surface of the specimen.

In this study, all LDTs had two strain gauges. The vertical LDTs were 0.3mm thick, 5mm wide and 70mm long. The horizontal LDTs were 0.3mm thick, 5mm wide and 60mm long. Local axial strains,

. 1, were measured using two local deformation transducers placed vertically on opposite sides of the specimen. Lateral strains, . 2, in the . 2 direction were measured using four LDTs placed horizontally on the . 3 surfaces, two on each side at different heights. Lateral strains, . 3. in the . 3 direction were measured using two pairs of proximeters and aluminium foil targets attached at two different heights on the . 3 surfaces. One external displacement transducer was used to measure overall axial strains externally. However, this external measurement might include bedding errors due to non-uniform contact of the specimen ends with the top cap and pedestal.

When the frozen specimen is covered with the membrane, the imprinted side of membrane by using black dots with a diameter of 0.8mm and at a spacing of 5mm was positioned over one of the . 2 surfaces of the specimen that would be in contact with the transparent plexiglass plate. The specimen was set in the cell and after thawing, the suction was increased to 49kPa. The cell was filled with water. Double vacuuming was employed to remove air from the specimen and cell water. In this process, the cell suction was increased to 49kPa and sample suction to 98kPa. Under this condition, the specimen was fully saturated for 1 hour. After that the cell suction was reduced to zero and sample suction to 49kPa. B value was then measured to confirm the degree of saturation. After this, the cell water was expelled, and the cell cover was removed. The specimen was left to undergo consolidation at a confining stress of 49kPa till the next day.

The two confining plates were set, and an initial setting stress, q_{2o}= . 2-. 3, of about 9.8kPa was applied to ensure good contact between the plates and specimen surface. The cell was connected to the axial loading system, and the specimen was sheared under drained condition.

TEST RESULTS AND DISCUSSION

Both monotonic and cyclic plane strain compression tests were performed. Figure 3 shows stress-strain relationships for two monotonic and two cyclic tests. It should be noted that in the cyclic tests, 20 or 50 cycles of vertical loading at an axial strain rate of 0.03%/min was applied from a neutral deviator stress q_0 of 135kPa (state b in Fig.3) with a single amplitude q_d of 103kPa followed by a monotonic loading at a strain rate of 0.01%/min. The monotonic tests were conducted under a constant axial strain rate of 0.01%/min.

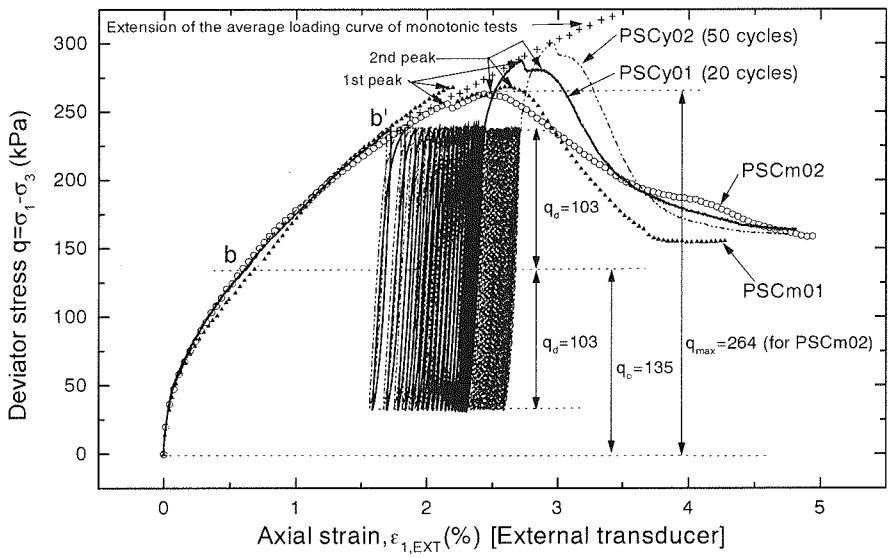

Figure 3 Stress-strain relationships for PSC monotonic and cyclic tests

In the cyclic tests, the maximum amplitude of cyclic loading $q=(q_o+q_d)$ was set at almost 90% of the average peak deviator stress q_{max} observed in monotonic tests. The minimum cyclic amplitude $q=(q_o-q_d)$ was set at almost 10% of q_{max}.

The two monotonic tests showed reasonable repeatability up to the peak stress states. The average value of q_{max} was 266 kPa. In addition, in these two monotonic tests, two local peaks with different deviator stress levels were observed. The two cyclic tests showed higher q_{max} values than the monotonic tests. These peak stress states in the cyclic tests seem to lie on the extension of the average stress-strain curve of monotonic tests as added in Fig. 3. The possible reason for the higher q_{max} values for large amplitude cyclic tests was local densification in the specimen during cyclic loading, as will be discussed in detail later. From the figure, it was observed that the cyclic test with 50 cycles produced higher q_{max} value than the cyclic test with 20 cycles. By this observation, it can be inferred that the more the number of cycles, the more the local densification and subsequently higher peak strength. The extension of the average stress-strain curve of monotonic tests added in the figure suggests that if the number of cycles is increased from 50, the peak strength would increase. Without the support of available data, it is not possible to conclude this with certainty, because a limit may exist when this behavior would cease to occur.

For all the tests shown in the Fig. 3, almost the same residual stress level was reached. One notable observation during the cyclic loading stage of the tests was that the overall axial strain increments after each cycle decreased with increase in the number of cycles. In the later stages of cyclic loading, the cycle loops overlapped to each other and it was difficult to distinguish visually the start and end of cycles. This is well illustrated in Fig. 4 where results from the two cyclic tests are shown. The overall axial strain increments per cycle were highest in the initial cyclic loading stage but decreased with further increase in number of cycles. Especially after the first cycle, large overall axial strain increments were noticed. They are associated with the large overall axial strain increments during the virgin loading in the monotonic loading tests (path b to b' in Fig. 3). A reasonable repeatability exists in the overall axial strain increments per cycle for the two cyclic tests.

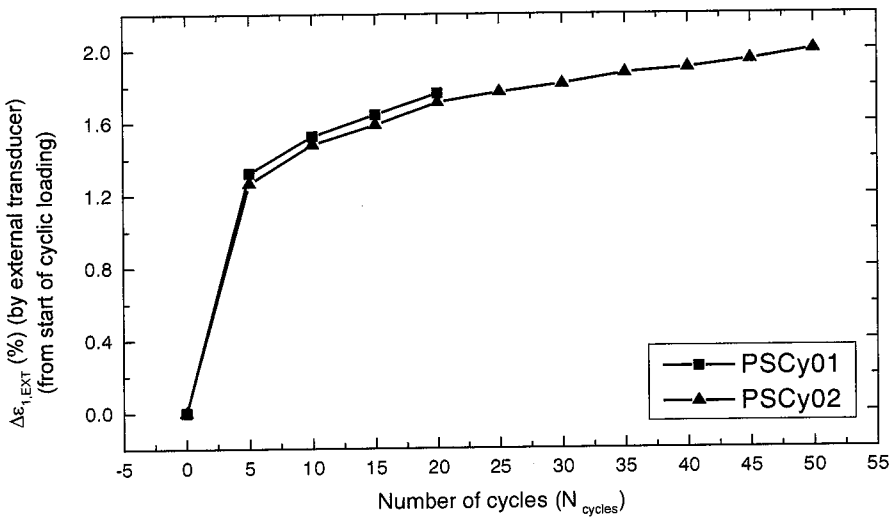

Figure 4 Overall axial strain increments with number of cycles

Strain localization characteristics on dense Toyoura sand

To study strain localization characteristics and their relation with the failure mechanism of dense Toyoura sand, maximum shear strain γ_{max} ($=\varepsilon_1-\varepsilon_3$) and volumetric strain increments . .vol (=. .1+. .3) distributions were calculated at different stages of loading. The apparatus used allows digital photographs of the specimen's σ_2 face to be taken through the transparent plexiglass plate and the

membrane used had been imprinted with a series of dots equally spaced every 5 mm. The horizontal and vertical displacements of each dot were read from the photographs taken at different stages during the test. From this data, the deformation at the center of each of the rectangular elements defined by the grid of dots was calculated. Finally, strain fields showing the strain throughout the specimen's face at each of the stages of loading were plotted.

Strain localization is important in this research to understand how failure and shear banding in particular, take place in dense Toyoura sand during shearing. The influence of large amplitude cyclic loading and creep loading on shear banding is investigated.

Monotonic plane strain compression tests

Figure 5 shows the contours of the maximum shear strains, γ_{max} ($=\varepsilon_1-\varepsilon_3$) at and after the peak stress states for one monotonic test obtained by the methods explained above. The γ_{max} value was defined to be zero at the isotropic stress state before vertical loading. Shear band formation was progressive and γ_{max} values accumulated rapidly in the shear band between the first and the second peaks.

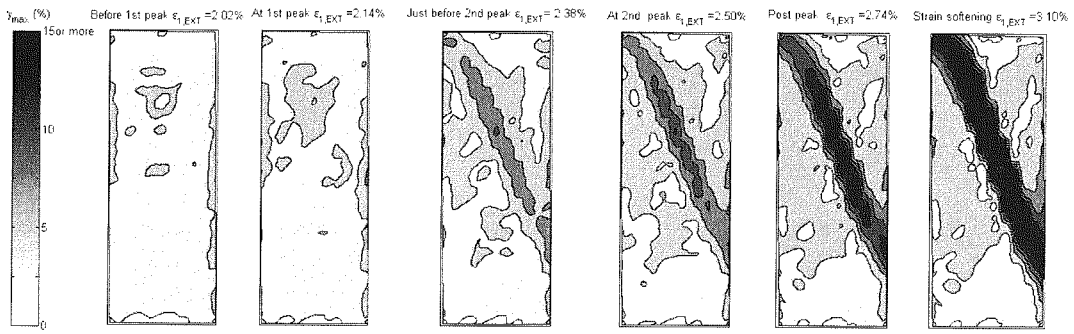

Figure 5 Contours of maximum shear strain at 2.5% intervals for monotonic test PSCm02

For the same monotonic test, contours of volumetric strain increments $\Delta\varepsilon_{vol}$ ($=\Delta\varepsilon_1+\Delta\varepsilon_3$) between several stress states are plotted in Fig. 6. The corresponding values of overall axial strain intervals are shown on top of each figure. Just after the first peak stress states, dilative regions ($\Delta\varepsilon_{vol}$ <-0.1%) were observed along the location of the final shear band. Except for this localization, contractive regions ($\Delta\varepsilon_{vol}$ >0.1%) were locally observed as well around the peak stress states, while their locations were not always fixed. It should be noted that, considering the accuracy of evaluating $\Delta\varepsilon_{vol}$ values, the regions with $\Delta\varepsilon_{vol}$ ranging between -0.1 and 0.1% were regarded as neither dilative nor contractive.

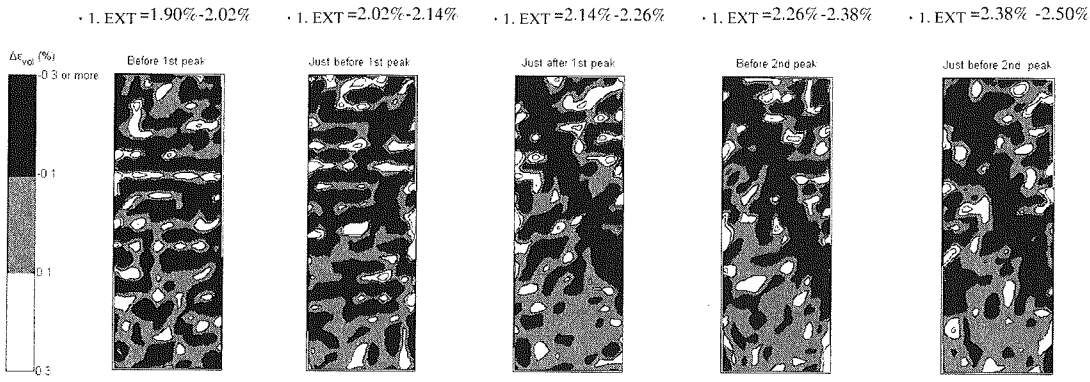

Figure 6 Contours of volumetric strain increments for monotonic test PSCm02

Cyclic plane strain compression tests

Figure 7 shows the contours of the maximum shear strains γ_{max} at two states during cyclic loading, and at three states during the subsequent monotonic loading for one cyclic test. In this test, shear band formation started after the first peak stress state during the latter monotonic loading stage. Although the value of the overall axial strain at the end of the cyclic loading was larger than 2.5%, at which shear band had been already formed in the monotonic test without cyclic loading, the location of final shear band was not evident at this strain level in the cyclic test.

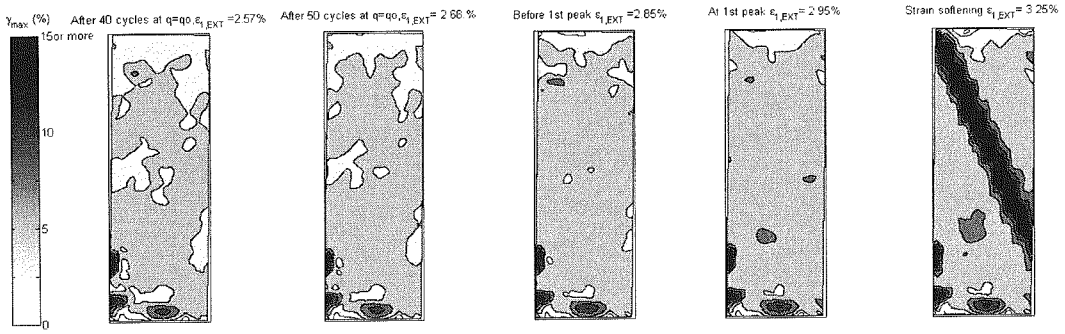

Figure 7 Contours of maximum shear strain at 2.5% intervals for cyclic test PSCy02

Contours of volumetric strain increments during cyclic loading are plotted in Fig. 8 for the same test as in Fig.7. With the increase in the number of cycles, contractive regions ($\Delta\varepsilon_{vol}$ >0.1%) expanded slightly, while dilative regions ($\Delta\varepsilon_{vol}$ <-0.1%) reduced significantly. When compared to the results from the monotonic test (Fig.6), less dilative behavior was observed in the cyclic tests. Such behavior suggests an occurrence of larger extent of local densification. It may be linked with the larger peak strengths in cyclic tests than in monotonic tests, since potentially weak zones due to the initial heterogeneity of specimen may have been strengthened by this local densification during cyclic loading.

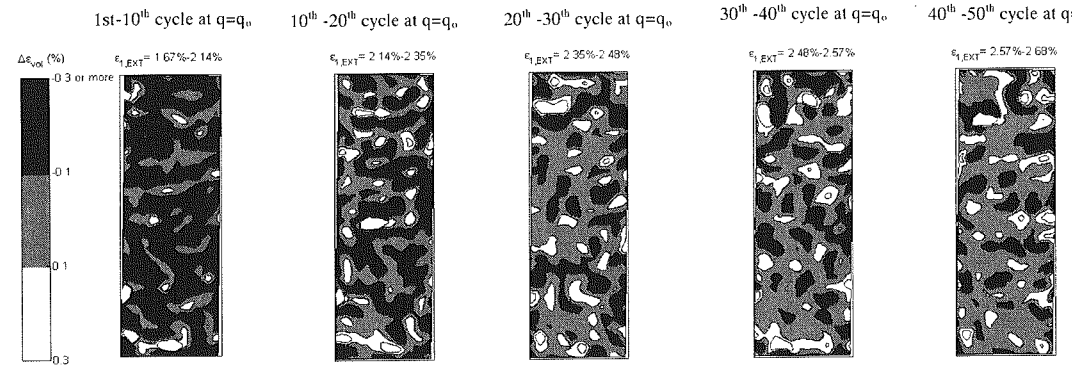

Figure 8 Contours of volumetric strain increments for cyclic test PSCy02

This behavior is clearly seen in Fig.9 where volumetric strains and volumetric strain increments based on the averaged values from image analysis were plotted against axial strains. At every cycle during cyclic loading, the volumetric strain increments were evaluated at the neutral deviator stress state $q=q_0$. As a result, negative volumetric strain increments increased rapidly during the first cycle, suggesting dilative

behavior. This rapid increase in dilation may be associated with the large axial strain increments during the virgin loading of the first quarter cycle. After the first cycle, the volumetric strain increments decreased sharply and later became constant (nearly zero) until the end of the cyclic loading. This decrease in the overall volumetric strain increments during the cyclic loading stage after the first cycle suggested an occurrence of local contraction or densification in the material.

During the final monotonic loading following the cyclic loading, as can be seen from the change in the increasing trend of negative volumetric strain, the material showed more dilative behavior. It should be noted that the volumetric strain increments during monotonic loading were evaluated at an interval of about 0.1 % in the axial strain increments, and thus they cannot be directly compared with those during cyclic loading that were obtained based on different definitions, as mentioned above.

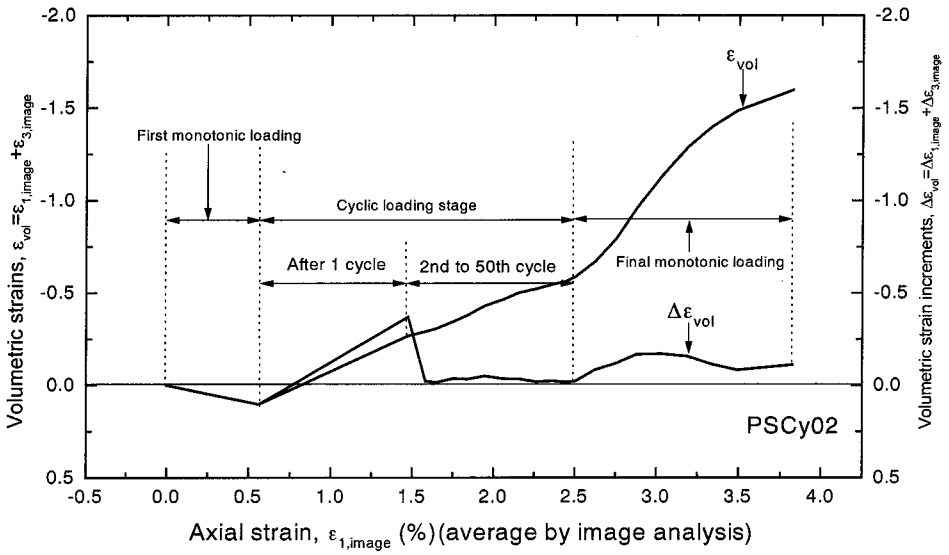

Figure 9 Average volumetric strains and their increments for cyclic test (PSCy02)

The aforementioned process of local densification during cyclic loading may have started with the weaker (looser) regions being strengthened (densified). This may have caused delayed initiation of strain localization. The end result was a higher maximum deviator stress (q_{max}) than in monotonic loading tests. It should be noted again that, the peak strength for the cyclic test with 50 cycles is more than the peak strength of the cyclic test with 20 cycles. Going by the local densification phenomenon, it implies that 50 cycles of loading subjected the specimen to more local densification than 20 cycles. It was not possible, however, to account for this difference in the amount of local densification for the two cyclic tests by volumetric strain increments distributions.

Creep plane strain compression tests

Figure 10 shows the combined stress-strain relationships for two creep tests and one monotonic test (PSCm02). The creep loading for PSCc02 was applied by keeping a constant deviator stress q_{creep} which was almost equal to the stress level at the maximum amplitude of cyclic loading $q=(q_o+q_d)$ in the large amplitude cyclic loading tests explained earlier. The creep loading was applied for duration of 210 minutes. For another creep test PSCc03, creep loading was applied for 230 minutes at a higher level of q_{creep} than in PSCc02. After creep loading, monotonic loading was applied for both tests. Immediately after the creep loading stage, an initial sharp increase in stiffness was observed. However, no significant change in their peak strengths was observed when compared with peak strength from the monotonic test.

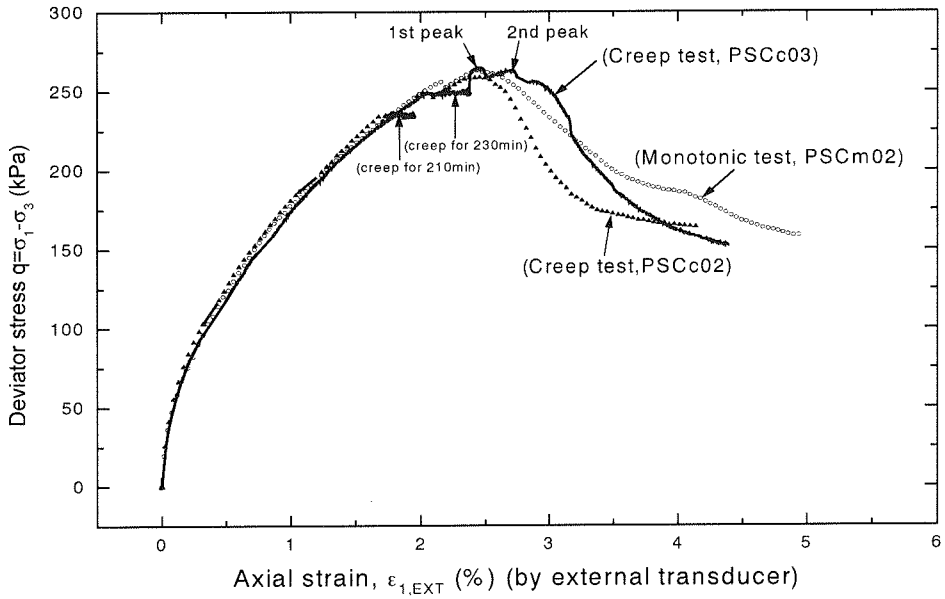

Figure 10 Stress-strain relationships for PSC monotonic and creep tests

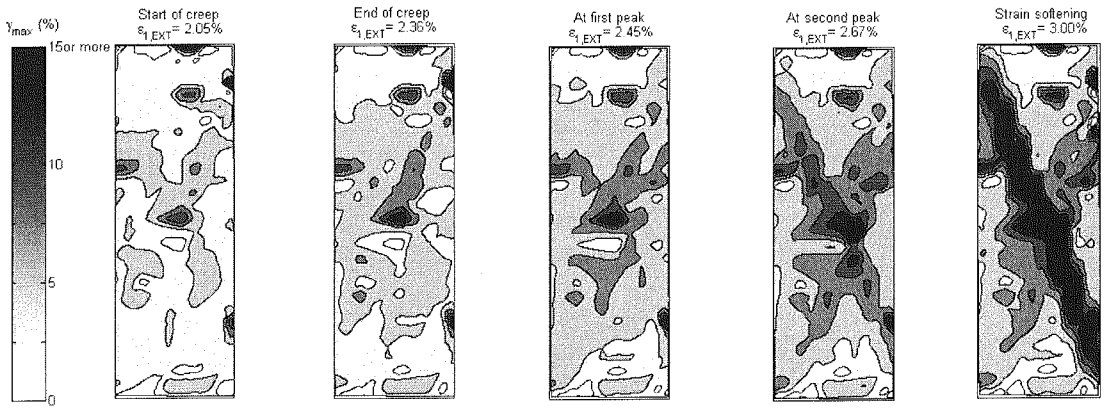

Figure 11 Contours of maximum shear strain at 2.5% intervals for creep test PSCc03

Strain localization properties during creep loading were studied to investigate the possible effect of creep loading on strength and deformation characteristics of dense Toyoura sand. In this paper, strain localization properties for PSCc03 will be presented for discussion.

Figure 11 shows the contours of the maximum shear strains γ_{max} (=ε_1-ε_3) during and after creep loading for PSCc03. At the start of creep loading in this particular test, some strain localization had already taken place due to initial monotonic loading. From the start to the end of creep loading, no significant change in terms of strain localization was observed. It is not known what would have happened if creep loading was applied for a longer period of time.

After restarting monotonic loading until the first peak stress state, strain continued to accumulate in the region where strain localization had already taken place. However, at the second peak stress state, strain accumulation stopped in this region and strain localization took place in another region where the final shear band was formed during strain softening regime. This could possibly explain why two peaks were formed in this creep loading test. That is, strain softening behavior after the first peak stopped when the strain localization in the first possible shear band stopped. Then strain localization started in another region, resulting in the formation of the second peak.

However, no such complicated strain localization behavior was observed in the other creep test (PSCc02). In the monotonic tests, where two local peaks were also observed, no such behavior on strain localization was observed either, as typically seen from Fig. 5.

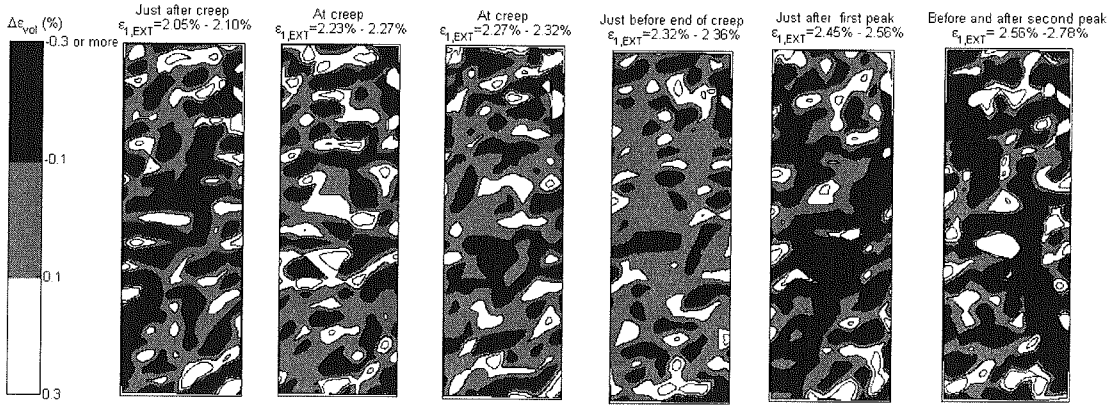

Figure 12 Contours of volumetric strain increments for creep test PSCc03

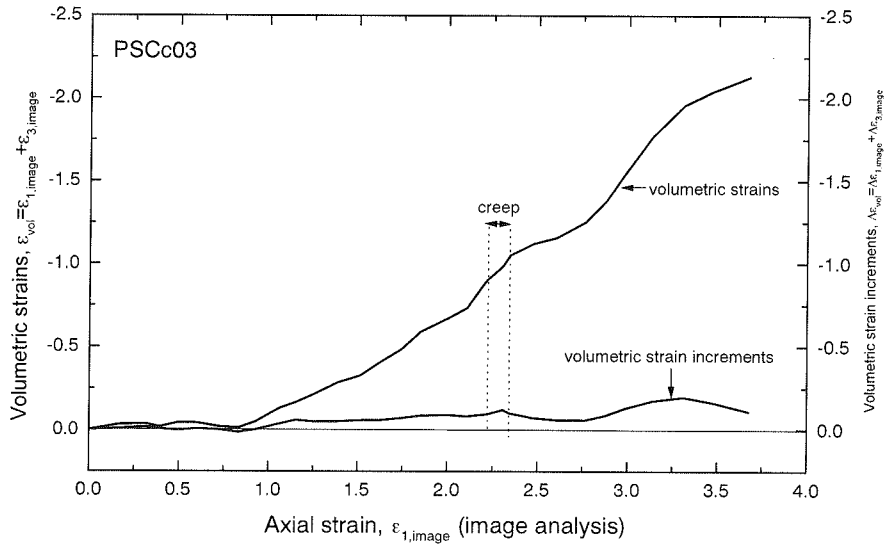

Figure 13 Average volumetric strains and their increments for creep test (PSCc03)

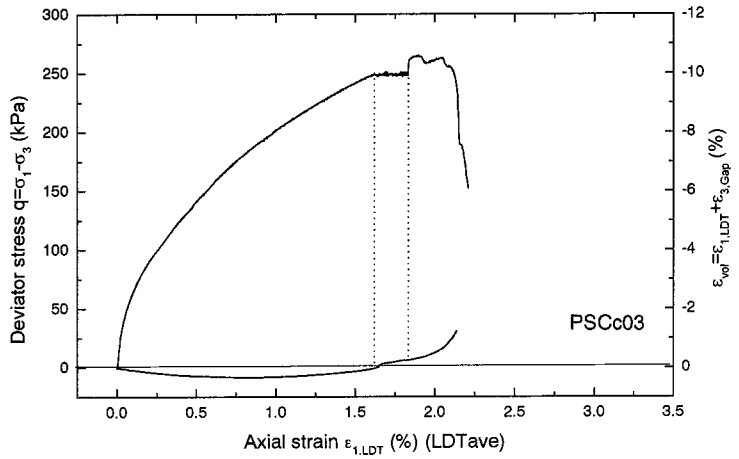

Figure 14 Stress-strain relationship for creep test PSCc03 and its volumetric strains

Figure 12 shows the contour graphs of volumetric strain increments for the same creep test (PSCc03). During creep loading, dilative regions decreased slightly, while contractive regions did not change significantly. Similarly, as can be seen from Fig. 13, the overall dilatancy property of the material based on the image analysis did not change significantly during creep loading. No significant change in the dalatancy property during creep loading was also observed in Fig. 14 where volumetric strains that were evaluated by vertical LDTs and horizontal gap sensors for the same creep test are shown. This may explain why creep loading had no effect on the peak strength of creep tests when compared with monotonic tests (Fig. 10).

CONCLUSIONS

The following conclusions can be drawn from the test results presented in this paper:

1. Under different loading mechanisms and at different stages of loading in plane strain compression tests on dense Toyoura sand, the accumulation of strains and in particular the progressive formation of shear band could easily be followed by analyzing strain distributions calculated from digital photographs.
2. In monotonic loading, uniform deformation was observed in the initial stages of loading and strain localization accumulated rapidly between first and second peak stress states. Shear band was formed in a progressive manner.
3. The initiation of shear band in large amplitude cyclic loading tests started after the first peak stress state at an overall axial strain level that was much larger than those in the monotonic tests. The peak strengths observed in cyclic tests were higher than those in monotonic tests.
4. During large amplitude cyclic loading, dilative regions reduced significantly while contractive regions expanded slightly, suggesting an occurrence of larger extent of local densification. It may be linked with the larger peak strengths in cyclic tests than in monotonic tests.
5. In large amplitude cyclic loading tests, the process of local densification during cyclic loading may have started with the weaker (looser) regions being strengthened (densified). This caused delayed initiation of strain localization. The end result was a higher maximum deviator stress (q_{max}) than in monotonic loading tests.
6. A change in the location of strain localization was observed in one of the creep tests after the first peak stress state.

7. No increase in peak strength was observed in specimens with creep loading history. This may be linked with the observation that their dilatancy property did not change significantly during creep loading, as compared to during cyclic loading.

ACKNOWLEDGEMENTS

The authors express their deep appreciations to Ms. Salas Monge, R. at Costa Rican Institute of Electricity and Ms. Tsutsumi, Y. at IIS, University of Tokyo for their help in conducting the image analysis.

REFERENCES

AnhDan L.Q., Koseki, J., and Sato, T. (2002) "Comparison of Young's moduli of dense sand and gravel measured by dynamic and static methods." *Geotechnical Testing Journal*, ASTM, Vol. 25, No. 4, 349-368.

Arthur, J.R.F. and Assadi, A. (1977). "Ruptured sand sheared in plane strain." *Proceedings of the 9th International Conference on Soil Mechanics and Foundation Engineering*, Tokyo, Vol.1, 19-22.

Koseki, J., Munaf, Y., Tatsuoka, F., Tateyama, M., Kojima, K. and Sato, T. (1998a) "Shaking and tilt table tests of geosynthetic-reinforced soil and conventional-type retaining walls." *Geosynthetic International*, Vol. 5, Nos. 1-2, 73-96.

Koseki, J., Tateyama, M., Horii, K., Munaf, Y. and Kojima, K. (1999) "Back analyses of case histories and model tests on seismic stability of retaining walls." *11th Asian Regional Conference on Soil Mechanics and Geotechnical Engineering*, Vol.1, 399-402.

Koseki, J., Tatsuoka, F., Munaf, Y., Tateyama, M. and Kojima, K. (1998b) "A modified procedure to evaluate active earth pressure at high seismic loads" *Soils and Foundations*, Special Issue on Geotechnical Aspects of the January 17 1995 Hyogoken-Nambu Earthquake, Vol. 2, 209-216.

Lam, W.K. and Tatsuoka, F. (1988). "Effects of initial anisotropic fabric and σ_2 on strength and deformation characteristics of sand." *Soils and Foundations*, Vol.26, No.1, 65-84.

Masuda, T., Tatsuoka, F., Yamada, S., and Sato, T. (1999). "Stress-strain behaviour of sand in plane strain compression, extension and cyclic loading tests" *Soils and Foundations,* Vol. 39, No. 5, 31-45.

Salas Monge, R., Koseki, J. and Sato, T. (2002) "Cyclic plane strain compression tests on cement treated sand" *Bulletin of Earthquake Resistant Structure Research Centre*, IIS, University of Tokyo, No. 36, 131-141.

Oda, M., Koishikawa, I. and Higuchi, T. (1978). "Experimental study of anisotropic shear strength of sand by plane strain test." *Soils and Foundations*, Vol.18, No.1, 25-38.

Tatsuoka, F. (1988), "Some recent developments in triaxial testing system for cohesionless soils", ASTM STP No.977, 7-67.

Tatsuoka, F., Koseki, J. and Tateyama, M. (1996) "Performance of reinforced soil structures during the 1995 Hyogo-ken Nanbu earthquake, Earth Reinforcement." Ochiai, Yasufuku & Omine (eds), A.A.Balkema, Vol. 2, 973-1008.

Tatsuoka, F., Nakamura, S., Huang, C.C. and Tani, K. (1990). "Strength anisotropy and shear band direction in plane strain tests of sand" *Soils and Foundations,* Vol. 30, No.1, 35-34.

Tatsuoka, F., Sakamoto, M., Kawamura, T., Fukushima, S. (1986). "Shear strength and deformation characteristics of sand in plane strain compression at extremely low pressures" *Soils and Foundations*, Vol. 26, No. 1, 65-84.

Watanabe, K., Munaf, Y., Koseki, J., Tateyama, K., Kojima, K. (2003) "Behaviours of several types of model retaining walls subjected to irregular excitation" *Soils and Foundations*, Vol. 43, No. 5, 13-27.

Yoshida, T., Tatsuoka, F., Siddiquee, M.S.A., Kamegai, Y. and Park, C.S. (1994). ''Shear banding in sands observed in plane strain compression" *Proceedings of the Third International Workshop on Strain Localization and Bifurcation Theory for Soils and Rocks,* Balkema,165-179.